Mon. Not. R. Astron. Soc. **388,** 347–356 (2008) doi:10.1111/j.1365-2966.2008.13393.x

The complex light curve of the afterglow of GRB 071010A⋆

S. Covino,[1]† P. D'Avanzo,[1,2] A. Klotz,[3,4] D. A. Perley,[5] L. Amati,[6] S. Campana,[1] G. Chincarini,[1,7] A. Cucchiara,[8] V. D'Elia,[9] D. Guetta,[9] C. Guidorzi,[1,7] D. A. Kann,[10] A. Küpcü Yoldaş,[11] K. Misra,[12,13] G. Olofsson,[14] G. Tagliaferri,[1] L. A. Antonelli,[9] E. Berger,[15] J. S. Bloom,[5] M. Böer,[3] C. Clemens,[11] F. D'Alessio,[9] M. Della Valle,[16,17,18] S. di Serego Alighieri,[19] A. V. Filippenko,[5] R. J. Foley,[5] D. B. Fox,[7] D. Fugazza,[1] J. Fynbo,[20] B. Gendre,[21] P. Goldoni,[22,23] J. Greiner,[11] D. Kocevksi,[5] E. Maiorano,[6] N. Masetti,[6] E. Meurs,[24,25] M. Modjaz,[5] E. Molinari,[1] A. Moretti,[1] E. Palazzi,[6] S. B. Pandey,[12] S. Piranomonte,[9] D. Poznanski,[5] N. Primak,[11] P. Romano,[1] E. Rossi,[26] R. Roy,[12] J. M. Silverman,[5] L. Stella,[9] G. Stratta,[27] V. Testa,[9] S. D. Vergani,[24,25] F. Vitali[9] and F. Zerbi[1]

[1]*INAF/Osservatorio Astronomico di Brera, via Bianchi 46, 23807 Merate, LC, Italy*
[2]*Università dell'Insubria, Dipartimento di Fisica e Matematica, via Valleggio 11, 22100 Como, Italy*
[3]*Observatoire de Haute-Provence, 04870 Saint-Michel l'Observatoire, France*
[4]*CESR, 9 Avenue colonel Roche, Université de Toulouse, 31400 Toulouse, France*
[5]*Astronomy Department, University of California, 445 Campbell Hall, Berkeley, CA 94720-3411, USA*
[6]*INAF/Istituto di Astrofisica Spaziale e Fisica Cosmica di Bologna, via Gobetti 101, 40129 Bologna, Italy*
[7]*Università degli Studi di Milano, Bicocca, Piazza delle Scienze 3, 20126 Milano, Italy*
[8]*Department of Astronomy and Astrophysics, Pennsylvania State University, USA*
[9]*INAF/Osservatorio Astronomico di Roma, via Frascati 33, 00040 Monteporzio Catone, Roma, Italy*
[10]*Thüringer Landessternwarte Tautenburg, Sternwarte 5, 07778 Tautenburg, Germany*
[11]*Max-Planck-Institut für extraterrestrische Physik, Giessenbachstrasse 1, 85748 Garching, Germany*
[12]*Aryabhatta Research Institute of Observational Sciences (ARIES), Manora Peak, Nainital 263129, India*
[13]*Inter University Centre for Astronomy and Astrophysics, Post Bag 4, Ganeshkhind, Pune 411007 India*
[14]*Stockholm Observatory, Roslagstullsbacken 21, 10691 Stockholm, Sweden*
[15]*Observatories of the Carnegie Institution of Washington, 813 Santa Barbara Street, Pasadena, CA 91101, USA*
[16]*INAF/Osservatorio Astronomico di Capodimonte, Via Moiariello 16, 80131 Napoli, Italy*
[17]*Icranet, International Centre for Relativistic Astrophysics Network, Piazza Repubblica 10, Pescara, Italy*
[18]*European Southern Observatory, Garching bei Munchen, Germany*
[19]*INAF/Osservatorio Astrofisica di Arcetri, Largo Enrico Fermi 5, 50125 Firenze, Italy*
[20]*Dark Cosmology Centre, Niels Bohr Institute, University of Copenhagen, Juliane Maries vej 30, 2100 Kobenhavn, Denmark*
[21]*Laboratoire d'Astrophysique de Marseille/CNRS/Université de Provence, 13376 Marseille Cedex 12, France*
[22]*Laboratoire Astroparticule et Cosmologie, 10 rue A. Domon et L. Duquet, 75205 Paris Cedex 13, France*
[23]*Service d'Astrophysique, DSM/DAPNIA/SAp, CEA-Saclay, 91191 Gif-sur-Yvette, France*
[24]*Dunsink Observatory – DIAS, 31 Fitzwilliam Street, Dublin 2, Ireland*
[25]*School of Physical Sciences and NCPST, Dublin City University, Dublin 9, Ireland*
[26]*JILA, University of Colorado, 440 UCB Boulder, CO 80309-0440, USA*
[27]*ASI Science Data Centre (ASDC), via G. Galilei, 00044 Frascati, Italy*

Accepted 2008 April 28. Received 2008 April 19; in original form 2008 February 21

ABSTRACT

We present and discuss the results of an extensive observational campaign devoted to GRB 071010A, a long-duration gamma-ray burst detected by the *Swift* satellite. This event was followed for almost a month in the optical/near-infrared (NIR) with various telescopes starting from about 2 min after the high-energy event. *Swift* XRT observations started only later at about 0.4 d. The light-curve evolution allows us to single out an initial rising phase

⋆Based on observations made also with ESO Telescopes at the La Silla and Paranal Observatory under programme IDs 080.D-0229, 080.D-0250 and 080.D-792.
†E-mail: stefano.covino@brera.inaf.it

with a maximum at about 7 min, possibly the afterglow onset in the context of the standard fireball model, which is then followed by a smooth decay interrupted by a sharp rebrightening at about 0.6 d. The rebrightening was visible in both the optical/NIR and X-rays and can be interpreted as an episode of discrete energy injection, although various alternatives are possible. A steepening of the afterglow light curve is recorded at about 1 d. The entire evolution of the optical/NIR afterglow is consistent with being achromatic. This could be one of the few identified GRB afterglows with an achromatic break in the X-ray through the optical/NIR bands. Polarimetry was also obtained at about 1 d, just after the rebrightening and almost coincident with the steepening. This provided a fairly tight upper limit of 0.9 per cent for the polarized-flux fraction.

Key words: methods: observational – gamma-rays: bursts – X-rays: individual: GRB 071010A.

1 INTRODUCTION

The *Swift* satellite (Gehrels et al. 2004) has revolutionized gamma-ray burst (GRB) science by introducing dedicated observational strategies and providing a wealth of high-quality data. In particular, a major breakthrough has been the spectral and temporal coverage at X-ray energies from a few minutes up to weeks or months after the GRB. This has provided unprecedented information on the late prompt and early afterglow evolution (Nousek et al. 2006). Optical observations from the ground, however, have not always been of comparable quality and late-time phases have been seldom monitored accurately (Covino et al. 2006). This is a consequence of the strong increase in the number of events to be followed, the large average redshift of *Swift* GRBs (Berger et al. 2006; Jakobsson et al. 2006), coupled with the difficulties in performing productive follow-up observations from the ground. While the early-time afterglow is often well sampled by the network of small and medium-class robotic telescopes around the world, the late-time afterglow can only be monitored with the largest instruments and only at the cost of significant observing time (Dai et al. 2007). Based on these considerations, we started a new program of afterglow observations with the explicit goal of providing full coverage of the optical/near-infrared (NIR) afterglow light curve for a selected number of events (building on visibility and availability of early-time observations) rather than providing sparse data points for most of the observable *Swift* GRBs.

The importance of dense temporal and spectral sampling is particularly crucial for the identification and interpretation of the different features in the light-curve evolution that are observed both in the optical (Kann et al. 2007) and at higher energies (Zhang & Mészáros 2004). In particular, in spite of intense observational efforts and continuous theoretical interest (e.g. Burrows & Racusin 2006; Covino et al. 2006; Dai et al. 2007; Curran et al. 2008; Dado, Dar & De Rujula 2008; Panaitescu 2008), the search for light-curve jet breaks fully satisfying the requirements of the standard fireball model, and thus allowing a correct inference of the true energy content of a GRB, is still far from complete (Liang et al. 2008).

The GRB 071010A afterglow evolution was followed in the optical by TAROT and in the NIR by REM and GROND at early times, then by Gemini-N, GROND, NOT, TNG, NTT, Keck-I, Sampurnanand and VLT in the subsequent two weeks. Multiband observations were acquired to study the temporal evolution of the afterglow spectral energy distribution (SED). A polarimetric observation was carried out almost in coincidence with a slope transition in the light curve. *Swift* XRT and BAT data were also studied. In Section 2 we report information about GRB 071010A, in Section 3 our observations, reductions, and data analysis are described, and in Section 4 a full discussion is presented. Our main conclusions are summarized in Section 5.

2 GRB 071010A

GRB 071010A was detected by *Swift* on 2007 October 10 at 03:41:12 (Moretti et al. 2007) (UT dates are used throughout this paper). The BAT light curve was relatively broad, with a T_{90} duration of 6 ± 1 s (a moderate-duration long GRB). The fluence was $(2.0 \pm 0.4) \times 10^{-7}$ erg cm^{-2} (uncertainty 90 per cent confidence, Krimm et al. 2007). Automatic slewing to the GRB position with the *Swift* narrow-field instruments was disabled, so the XRT observations were delayed by 34 ks (Guidorzi et al. 2007b). The optical afterglow was promptly identified by TAROT ($\alpha_{J2000} = 19{:}12{:}14.624$, $\delta_{J2000} = -32{:}24{:}07.16$; Bloom et al. 2007), revealing an initial flux increase up to about 470 s after the high-energy event, followed by a regular decay (Klotz, Böer & Atteia 2007a,b). Spectroscopy was carried out with Keck (Prochaska et al. 2007), revealing a strong Mg II absorber and corresponding Fe II lines at redshift $z \approx 0.98$. A refined analysis was carried out by D'Elia et al. (in preparation), deriving $z = 0.985 \pm 0.005$ (1σ error) for the absorbing system with the highest redshift. Lines of Mg II (2796–2803 Å), Mg I (2852 Å), Si II (2336 Å), Fe II (2367, 2374, 2586, 2600 Å), and Mn II (2594, 2606 Å) were identified. The afterglow was not detected in the radio band at 8.46 GHz almost two days after the GRB (Chandra & Frail 2007). Late-time observations led Perley et al. (2007) to suggest that the afterglow decay underwent a (possibly achromatic) steepening about one day after the burst. Galactic dust absorption along the GRB line of sight is $E_{B-V} \approx 0.098$ mag (Schlegel, Finkbeiner & Davis 1998).

Throughout this paper, the time decay and energy spectral indices α and β are defined by $F(t, \nu) \propto (t - t_0)^{-\alpha}\ \nu^{-\beta}$, where t_0 is the trigger time of the burst. We assume a ΛCDM cosmology with $\Omega_m = 0.27$, $\Omega_\Lambda = 0.73$ and $h_0 = 0.71$. At the redshift of the GRB the luminosity distance is 6.6 Gpc ($\sim 2.0 \times 10^{28}$ cm), corresponding to a distance modulus $\mu = 44.1$ mag. All uncertainties are 1σ unless stated otherwise.

3 OBSERVATIONS, REDUCTIONS AND ANALYSIS

3.1 Observations and reduction

The afterglow of GRB 071010A was observed by the TAROT telescope (Bringer et al. 1999) with the white and red filters, by the

REM telescope (Zerbi et al. 2001) equipped with the REMIR NIR camera (Vitali et al. 2003; Conconi et al. 2004), and by the 2.2-m MPI/ESO telescope equipped with GROND (Greiner et al. 2008) starting from 124 s after the GRB (86 s after reception of the GCN alert). The observations began at an initial airmass of about 2.3 with the target already setting. In order to obtain an acceptable signal-to-noise ratio (S/N) we needed to bin the REM data, thus decreasing the highest time resolution afforded by the instrument. Later NIR observations were carried out with Gemini-N equipped with NIRI, the TNG equipped with NICS, and the NTT equipped with SofI. In the optical the afterglow was again observed a few hours after the GRB with the Keck-I telescope equipped with LRIS, the Sampurnanand telescope, the NOT equipped with PolCor, and the VLT with FORS1 and FORS2. Polarimetry was carried out with the VLT equipped with FORS1 on 2007 October 11 at 1:11:33 (0.89607 d after the GRB) with a total exposure time of 1800 s.

Data reduction was carried out following standard recipes with the *Eclipse* package (Devillard 1997). Photometry was computed by aperture and profile-fitting photometry with the DAOPHOT (Stetson 1987) and SExtractor (Bertin & Arnouts 1995) packages. Photometric calibration was derived from the observation of standard stars in the optical on two different nights and with the 2MASS catalogue (Strutskie et al. 2006) in the NIR, although in a few cases the small field of view of NIR detectors made the calibration more difficult. TAROT data were calibrated with observations of two field stars and final magnitudes are expressed in the R2 system of the USNO-B1 catalogue (Monet et al. 2003). The results from the photometric observations are reported in Table 1.

For polarimetry, the offset between instrumental and intrinsic polarization was fixed by the observation of a polarized standard star. Instrumental polarization was derived by observation of non-polarized stars. The procedure we followed for the analysis of the FORS1 polarization data was extensively discussed by Covino et al. (1999, 2002, 2003). At the time of the observation the afterglow optical emission was consistent with null polarization with a 95 per cent upper limit of 0.9 per cent (1.3 per cent at 3σ) for the degree of polarized flux.

The *Swift* XRT data were reduced using the xrtpipeline task (v.0.9.9), applying standard calibration and filtering criteria, i.e. we cut out temporal intervals in which the CCD temperature was above $-47\,^{\circ}$C and removed hot and flickering pixels. An onboard event threshold of $\sim$0.2 keV was applied to the central pixel; this was proven to reduce most of the background due to the bright Earth and/or CCD dark current. We selected XRT grades 0–12 for data all in PC mode. A circular region of 20 pixel radius was selected for source extraction. Physical ancillary response files were generated using the task xrtmkarf. Optical/NIR and X-ray light curves are shown in Fig. 2.

The *Swift* BAT data were also analysed. The 15–150 keV mask-weighted energy spectrum was extracted with the FTOOL batbinevt using the BAT refined position (Krimm et al. 2007). All the required corrections were applied: we accounted for the slewing through the FTOOL batupdatephakw and produced the detector-response matrix with *batdrmgen*. The spectrum was corrected for systematics depending on energy with the FTOOL batphasyserr and was finally grouped by imposing a 3σ threshold on each grouped energy channel.

3.2 Analysis

The optical/NIR light curve is complex, with an initial rising phase, a maximum, then a decay interrupted by a rather sharp rebrightening, followed by a final steepening. We choose to fit the light curve with a Beuermann function (equation 1, Beuermann et al. 1999) for the first part down to the rebrightening:

$$F(t) = A/[(t/t_{\rm b})^{\kappa\alpha_{\rm r}} + (t/t_{\rm b})^{\kappa\alpha_{\rm d}}]^{1/\kappa}, \quad (1)$$

where A is a normalization constant, $\alpha_{\rm r(d)}$ is the slope of the rise (decay) phase, and κ is a smoothness parameter. The time at which the curve reaches its maximum is $t_{\rm max} = t_{\rm b}(-\alpha_{\rm r}/\alpha_{\rm d})^{1/[\kappa(\alpha_{\rm d}-\alpha_{\rm r})]}$.

We model the rebrigthening at about 0.6 d with a simple step function. We also tried more complex models by using a pulse following the functional form discussed in Norris, Nemiroff & Bonnell (1996) and in Guidorzi et al. (2007a). The quality of data did not allow us to study the transition in detail; we report the results requiring the minimum number of free parameters. A general discussion is given in Section 4.

The later time evolution of the afterglow shows a final steepening, and this was also modelled with a Beuermann function (equation 1). Both for the onset and the final steepening the transition from the first to the second power-law behaviour was remarkably sharp and the Beuermann's smoothness parameter had a high value ($\kappa \geq 10$, frozen in the fits), making the model essentially consistent with what would be obtained by using simple power-law segments. The temporal decay shown by the *Swift* XRT data was modelled with the same functional form as the optical/NIR where quasi-simultaneous data were available.

The data were fitted both in the spectral and temporal domains. The optical/NIR afterglow spectrum was modelled with a simple power law. Galactic dust absorption was removed and rest-frame absorption was modelled with the absorption curves of the Milky Way (MW), the Large and Small Magellanic Clouds (LMC, SMC) (Pei 1992), and for a starburst galaxy (SB) (Calzetti et al. 2000). For the I band we also added a constant component, possibly the host galaxy or a supernova (SN), as late-time data (later than about 10 d) show a clear flattening. However, the presence of a red point-like object $\sim$1 arcsec east of the afterglow, with $R = 23.22 \pm 0.06$ mag and $I = 22.31 \pm 0.07$ mag, makes late-time photometry less reliable (see Fig. 1). This source could also contribute to the NIR flux at about 2.8 d, when the observing conditions did not allow a reliable separation. A simple extrapolation to the NIR bands for $R - K \approx 1$ mag would suggest that it could be comparable in brightness to the afterglow. We therefore did not consider these data in the fits.

The model gives an acceptable fit ($\chi^2_{\rm d.o.f.} = 114.1/90 \approx 1.27$), particularly if one considers the number of telescopes contributing the data set under different observing conditions, filters, etc. A summary of the best-fitting parameters is reported in Table 2.

The early-time observations by TAROT, REM, and GROND allowed us to identify a rising phase, a maximum, and then a regular decay phase. The fit yields $t_{\rm max} = 420^{+124}_{-85}$ s ($\sim$7 min), $\alpha_{\rm r} = -0.88^{+0.43}_{-0.62}$, and $\alpha_{\rm d1} = 0.71^{+0.03}_{-0.04}$, for the time of the maximum and the rising and decaying power-law indices, respectively, in substantial agreement with the findings reported by Klotz et al. (2007b). The data do not suggest the presence of any spectral evolution.

A rebrightening peaking at about 0.6 d dominates the afterglow at intermediate times. The required flux ratio increase ($\sim$1.9) is remarkably high and, within the uncertainties, the same in the optical/NIR and X-rays. The later evolution of the afterglow requires a break, consistent with being fully achromatic in the optical/NIR and X-ray bands, at $t_{\rm break} = 0.96^{+0.09}_{-0.09}$ d, with a post-break decay index of $\alpha_{\rm d2} = 2.07^{+0.08}_{-0.07}$, followed by a final flattening likely due to the contribution from the GRB host galaxy. The best-fitting model is shown superposed on the data in Fig. 2.

Table 1. Optical/NIR observations of GRB 071010A. The reference time t_{GRB} is 2007 October 10, at 03:41:12 (Moretti et al. 2007). Data are not corrected for dust absorption. For the TAROT data, the 'clear' magnitudes are calibrated against the *R* filter. Data are sorted according to wavelength and according to time for each filter.

Mean date (UT)	$t - t_{GRB}$ (d)	Exposure time (s)	Airmass	Filter	Instrument	Magnitude
2007 October 11.036 01	0.882 40	60 × 2	1.2	*U*	VLT+FORS2	20.77 ± 0.07
2007 October 12.011 51	1.857 90	60 × 1	1.1	*U*	VLT+FORS2	22.11 ± 0.13
2007 October 11.039 45	0.885 84	60 × 2	1.2	*B*	VLT+FORS2	21.16 ± 0.04
2007 October 12.021 97	1.868 36	60 × 5	1.1	*B*	VLT+FORS2	22.75 ± 0.05
2007 October 10.840 27	0.686 66	0.1 × 6000	3.9	*V*	NOT+PolCor	20.20 ± 0.09
2007 October 11.033 76	0.880 15	40 × 1	1.2	*V*	VLT+FORS1	20.35 ± 0.04
2007 October 11.038 80	0.885 19	225 × 1	1.2	*V*	VLT+FORS1	20.34 ± 0.04
2007 October 11.041 64	0.888 03	60 × 1	1.2	*V*	VLT+FORS2	20.35 ± 0.04
2007 October 11.041 88	0.888 27	225 × 1	1.2	*V*	VLT+FORS1	20.36 ± 0.04
2007 October 11.044 96	0.891 35	225 × 1	1.2	*V*	VLT+FORS1	20.36 ± 0.04
2007 October 11.048 04	0.894 43	225 × 1	1.2	*V*	VLT+FORS1	20.37 ± 0.04
2007 October 11.051 35	0.897 74	225 × 1	1.2	*V*	VLT+FORS1	20.39 ± 0.04
2007 October 11.054 41	0.900 80	225 × 1	1.3	*V*	VLT+FORS1	20.40 ± 0.04
2007 October 11.057 48	0.903 87	225 × 1	1.3	*V*	VLT+FORS1	20.40 ± 0.04
2007 October 11.060 56	0.906 95	225 × 1	1.2	*V*	VLT+FORS1	20.42 ± 0.04
2007 October 11.209 25	1.055 64	180 × 1	1.7	*V*	Keck_I+LRIS	20.62 ± 0.04
2007 October 11.212 38	1.058 77	180 × 1	1.7	*V*	Keck_I+LRIS	20.62 ± 0.04
2007 October 12.026 82	1.873 21	60 × 2	1.1	*V*	VLT+FORS2	21.94 ± 0.04
2007 October 13.008 48	2.854 87	60 × 2	1.1	*V*	VLT+FORS2	22.75 ± 0.04
2007 October 10.201 07	0.047 45	100 × 1	1.7	*R*	Keck_I+LRIS	18.15 ± 0.06
2007 October 10.203 51	0.049 90	100 × 1	1.7	*R*	Keck_I+LRIS	18.25 ± 0.04
2007 October 10.285 70	0.132 09	120 × 1	2.2	*R*	Keck_I+LRIS	18.94 ± 0.04
2007 October 10.288 84	0.135 23	30 × 1	2.3	*R*	Keck_I+LRIS	18.98 ± 0.04
2007 October 10.292 30	0.138 69	30 × 1	2.3	*R*	Keck_I+LRIS	18.97 ± 0.04
2007 October 10.293 75	0.140 14	30 × 1	2.4	*R*	Keck_I+LRIS	18.98 ± 0.04
2007 October 10.295 30	0.141 69	30 × 1	2.4	*R*	Keck_I+LRIS	19.00 ± 0.04
2007 October 10.580 79	0.427 19	300 × 4	2.3	*R*	Sampurnanand	20.00 ± 0.20
2007 October 11.043 11	0.889 50	60 × 1	1.2	*R*	VLT+FORS2	19.78 ± 0.04
2007 October 11.067 35	0.913 74	180 × 1	1.3	*R*	VLT+FORS1	19.83 ± 0.04
2007 October 11.199 98	1.046 37	30 × 1	1.7	*R*	Keck_I+LRIS	20.05 ± 0.04
2007 October 11.201 62	1.048 01	30 × 1	1.7	*R*	Keck_I+LRIS	20.01 ± 0.05
2007 October 11.203 47	1.049 86	45 × 1	1.7	*R*	Keck_I+LRIS	20.03 ± 0.04
2007 October 11.205 82	1.052 21	45 × 1	1.7	*R*	Keck_I+LRIS	20.04 ± 0.04
2007 October 12.029 61	1.876 00	60 × 1	1.1	*R*	VLT+FORS2	21.34 ± 0.04
2007 October 13.014 53	2.860 92	60 × 5	1.1	*R*	VLT+FORS2	22.14 ± 0.04
2007 October 14.009 19	3.855 58	60 × 5	1.1	*R*	VLT+FORS2	22.87 ± 0.05
2007 October 16.018 41	5.864 80	60 × 15	1.2	*R*	VLT+FORS2	23.80 ± 0.08
2007 October 16.209 48	6.055 86	3 × 150	1.7	*R*	Keck_I+LRIS	24.03 ± 0.05
2007 October 10.827 11	0.673 50	0.1 × 6000	3.2	*I*	NOT+PolCor	18.81 ± 0.05
2007 October 11.044 57	0.890 96	60 × 1	1.2	*I*	VLT+FORS2	19.14 ± 0.03
2007 October 12.032 23	1.878 62	60 × 2	1.2	*I*	VLT+FORS2	20.65 ± 0.03
2007 October 14.015 44	3.861 83	60 × 5	1.1	*I*	VLT+FORS2	22.23 ± 0.05
2007 October 16.015 65	5.862 04	60 × 15	1.1	*I*	VLT+FORS2	23.06 ± 0.10
2007 October 27.000 14	16.846 53	180 × 3	1.2	*I*	VLT+FORS2	24.41 ± 0.29
2007 November 11.014 43	30.860 82	180 × 9	1.5	*I*	VLT+FORS2	24.44 ± 0.25
2007 October 10.157 42	0.003 81	10 × 5	2.3	*J*	REM+REMIR	14.72 ± 0.18
2007 October 10.164 98	0.011 37	30 × 5	2.5	*J*	REM+REMIR	15.08 ± 0.13
2007 October 10.167 37	0.013 76	240	2.5	*J*	GROND	15.16 ± 0.11
2007 October 10.178 56	0.024 95	60 × 5	3.0	*J*	REM+REMIR	15.64 ± 0.13
2007 October 10.264 26	0.110 53	30 × 9	2.0	*J*	GEMINI_N+NIRI	16.90 ± 0.05
2007 October 11.152 18	0.998 56	1200	2.2	*J*	GROND	17.76 ± 0.10
2007 October 13.010 86	2.857 26	60 × 15	1.1	*J*	NTT+SofI	19.90 ± 0.08
2007 October 10.155 19	0.001 58	10 × 5	2.3	*H*	REM+REMIR	14.43 ± 0.15
2007 October 10.160 38	0.006 77	30 × 5	2.4	*H*	REM+REMIR	14.02 ± 0.10
2007 October 10.167 37	0.013 76	240	2.5	*H*	GROND	14.38 ± 0.05
2007 October 10.170 49	0.016 88	60 × 5	2.8	*H*	REM+REMIR	14.52 ± 0.10
2007 October 10.272 97	0.119 36	60 × 12	2.1	*H*	GEMINI_N+NIRI	16.12 ± 0.05
2007 October 10.820 59	0.666 98	60 × 30	2.1	*H*	TNG+NICS	16.62 ± 0.04
2007 October 11.152 18	0.998 56	1200	2.2	*H*	GROND	16.94 ± 0.05
2007 October 13.048 76	2.895 15	60 × 20	1.2	*H*	NTT+SofI	19.01 ± 0.07
2007 October 10.156 32	0.002 71	10 × 5	2.3	*K*	REM+REMIR	13.42 ± 0.20

Table 1 – *continued*

Mean date (UT)	$t - t_{\rm GRB}$ (d)	Exposure time (s)	Airmass	Filter	Instrument	Magnitude
2007 October 10.162 70	0.009 09	30 × 5	2.4	*K*	REM+REMIR	13.39 ± 0.12
2007 October 10.167 37	0.013 76	240	2.5	*K*	GROND	13.66 ± 0.07
2007 October 10.174 55	0.020 94	60 × 5	2.8	*K*	REM+REMIR	14.04 ± 0.14
2007 October 10.289 11	0.135 50	30 × 6	2.3	*K*	GEMINI_N+NIRI	15.31 ± 0.05
2007 October 11.152 18	0.998 56	1200	2.2	*K*	GROND	16.10 ± 0.05
2007 October 13.027 86	2.874 25	60 × 25	1.1	*K*	NTT+SofI	18.20 ± 0.06
2007 October 10.155 23	0.001 61	31	2.3	Clear	TAROT	17.57 ± 0.15
2007 October 10.155 64	0.002 03	29	2.3	Clear	TAROT	17.20 ± 0.10
2007 October 10.157 93	0.004 32	90	2.3	Clear	TAROT	16.52 ± 0.10
2007 October 10.159 04	0.005 43	90	2.3	Clear	TAROT	16.39 ± 0.10
2007 October 10.160 23	0.006 61	91	2.3	*R*	TAROT	16.60 ± 0.10
2007 October 10.161 38	0.007 77	90	2.4	Clear	TAROT	16.68 ± 0.10
2007 October 10.162 49	0.008 88	89	2.4	Clear	TAROT	16.82 ± 0.10
2007 October 10.163 67	0.010 06	89	2.5	*R*	TAROT	16.97 ± 0.10
2007 October 10.164 84	0.011 23	90	2.5	Clear	TAROT	17.00 ± 0.10
2007 October 10.165 95	0.012 34	91	2.5	Clear	TAROT	17.10 ± 0.10
2007 October 10.167 14	0.013 53	90	2.5	*R*	TAROT	17.03 ± 0.10
2007 October 10.168 29	0.014 68	90	2.6	Clear	TAROT	17.20 ± 0.10
2007 October 10.169 40	0.015 79	90	2.6	Clear	TAROT	17.16 ± 0.10
2007 October 10.170 59	0.016 98	91	2.6	*R*	TAROT	17.27 ± 0.12
2007 October 10.186 39	0.032 78	365	3.3	Clear	TAROT	17.91 ± 0.12
2007 October 10.192 98	0.039 36	365	3.6	Clear	TAROT	17.98 ± 0.12

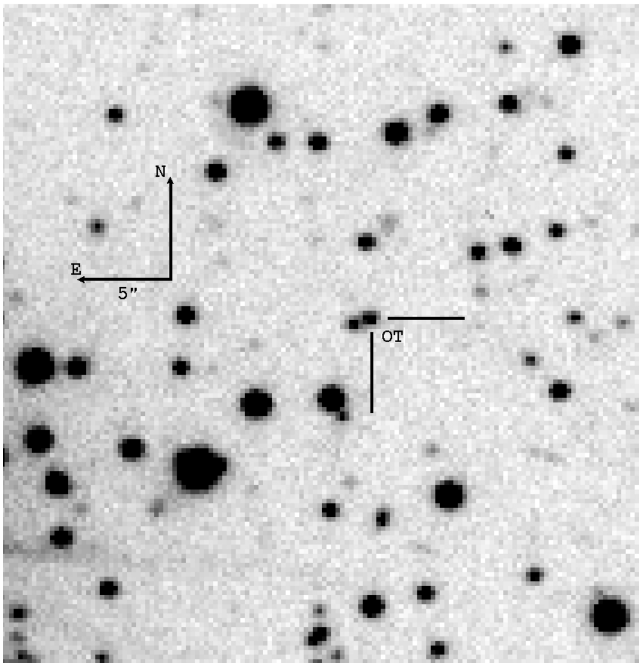

Figure 1. The field of GRB 071010A at about 3.8 d after the GRB in the *R* band observed with the VLT equipped with FORS 2. A nearby source at $R = 23.22 \pm 0.06$ at about one arcsec eastward of the afterglow is visible (see Section 3). The seeing of the image is ∼0.7 arcsec.

The entire afterglow spectral evolution is consistent with being achromatic. In the optical/NIR the broad-band SED index is $\beta = 0.76^{+0.23}_{-0.26}$, with a sizeable rest-frame extinction $E_{B-V} = 0.21^{+0.05}_{-0.05}$ mag after having removed the Milky Way absorption along the line of sight. Among the various extinction curves, only that of the SMC gave satisfactory results. The redshift of GRB 071010A would move the 2175-Å bump (see Fynbo et al. 2007, for a discussion about observations of this feature in GRB afterglow spectra), typical of Milky Way absorption (Pei 1992), into the *B* band, therefore easily detectable, if present, in our data sets.

Table 2. Best-fitting parameters.

Parameter	Interval
$\alpha_{\rm r}$	$-0.88^{+0.43}_{-0.62}$
$t_{\rm max}$	420^{+124}_{-85} s
$\alpha_{\rm d1}$	$0.71^{+0.03}_{-0.04}$
$t_{\rm break}$	$0.96^{+0.09}_{-0.09}$ d
$\alpha_{\rm d_2}$	$2.07^{+0.08}_{-0.07}$
$f_{\rm inj}/f$	∼1.9
$\beta_{\rm opt/NIR}$	$0.76^{+0.23}_{-0.26}$
E_{B-V}	$0.21^{+0.05}_{-0.05}$
$\beta_{\rm X}$	$1.46^{+0.22}_{-0.18}$
$N_{\rm H}$	$1.74(^{+0.57}_{-0.37}) \times 10^{22}$ cm^{-2}

The X-ray spectrum was modelled assuming a simple power law with neutral absorption in the Milky Way and in the host galaxy. Analysis of the hardness ratio showed that there are no significant spectral variations during the X-ray observations. The spectral analysis of the X-ray data alone ($\chi^2_{\rm d.o.f.} = 14.4/19 \approx 0.76$) provided satisfactory results. Fixing the Galactic absorption at 6.5×10^{20} cm^{-2} (Dickey & Lockman 1990) the rest-frame absorption and the spectral index turned out to be $1.74(^{+0.57}_{-0.37}) \times 10^{22}$ cm^{-2} and $\beta = 1.46^{+0.22}_{-0.18}$, respectively. The optical/NIR and X-ray spectral indices are consistent within the uncertainties with $\beta_{\rm X} \approx \beta_{\rm opt} + 0.5$, i.e. with the cooling break between the two bands. The broad-band SED is shown in Fig. 3.

The prompt time-averaged spectrum of GRB 071010A in the *Swift* BAT 15–150 keV energy band is consistent with a single power law with photon index significantly higher than 2 (Krimm et al.

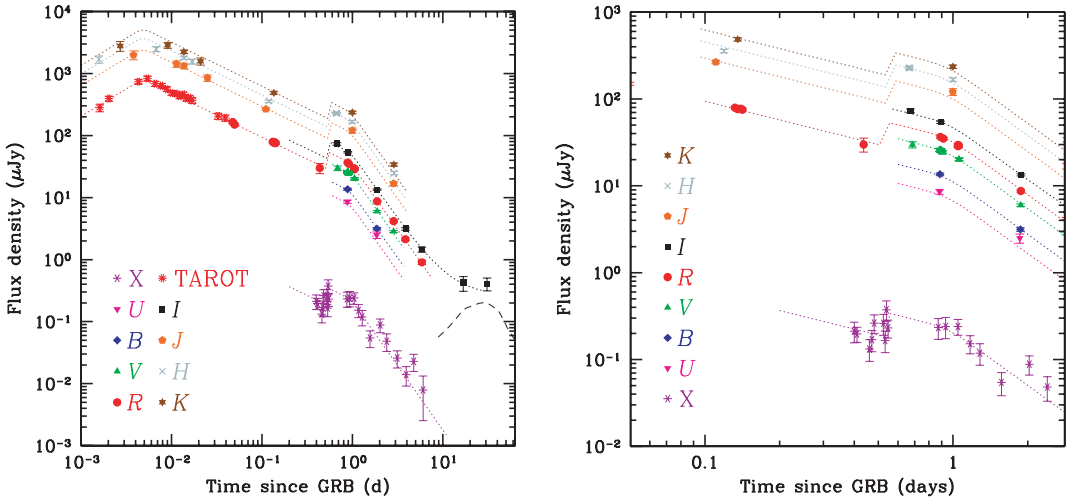

Figure 2. The optical, NIR and X-ray light curves of the afterglow of GRB 071010A. The dashed lines show the fit to the temporal decay of the early and late-time afterglow. Fit parameters are reported in Section 3. On the left-hand side we show the whole light curve fitted with the adopted model. On the right-hand side the epoch around 1 d is magnified. At late times, the long-dashed line shows the possible contribution to the *I* band by an SN component using SN 1998bw (Galama et al. 1998) as a template, at the redshift of GRB 071010A. The effect of the absorption in the optical is included.

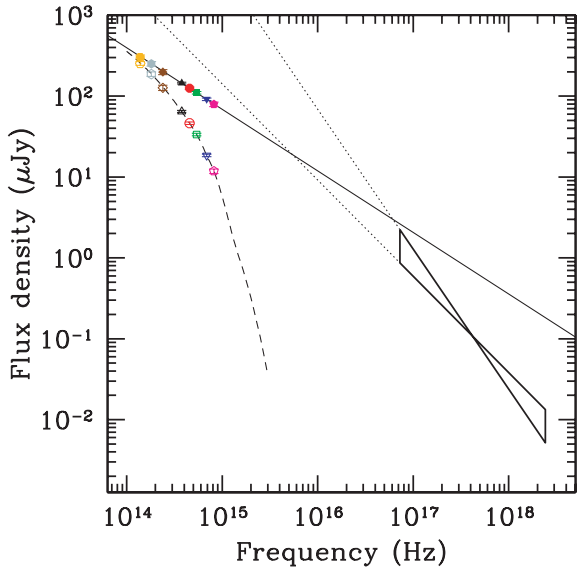

Figure 3. SED of the afterglow of GRB 071010A about 0.8 d after the burst. The dashed line is a fit to the observed data in the optical/NIR. The solid line refers to the intrinsic SED once the effect of dust absorption in the Milky Way and in the GRB host galaxy is removed. The X-ray and optical/NIR broad-band SED is consistent with the predictions of the synchrotron external-shock scenario with a cooling break between the optical/NIR and the X-ray and $\beta_X = \beta_{opt} + 1/2$.

2007), suggesting that the peak energy, E_{peak}, of this event is close to, or below, 20–30 keV. In order to better investigate this issue, we reduced and analysed the BAT time-averaged spectrum. The fit with a simple power law yields a photon index of 3.1 ± 0.7, confirming that GRB 071010A is a soft event, an X-ray flash (XRF). By fitting the spectrum with a Band function (Band et al. 1993) with α fixed at -1, we derive an upper limit to the peak energy E_{peak} of $\sim$35 keV, which corresponds to $\sim$70 keV in the GRB cosmological rest frame. Then, by varying E_{peak} from its upper limit to 0 and adopting the method of Ghirlanda, Ghisellini & Lazzati (2004) and Amati (2006), we estimated an isotropic-equivalent radiated energy in the 1–10000 keV cosmological rest-frame energy band, E_{iso}, of $(3.6 \pm 2.9) \times 10^{51}$ erg.

4 DISCUSSION

4.1 The onset

The temporal resolution of the observations does not allow us to check in detail the early-time density profile of the circumburst medium or possible chromaticity in the evolution. The modest duration of the prompt event and the late onset time argues against a scenario with frequent multiple peaks as for GRB 070311 (Guidorzi et al. 2007a). A smooth rising phase can also be produced by a decreasing extinction in the case of a radially decreasing circumburst density (Rykoff et al. 2004). However, the detection of the afterglow in the *U* band (Table 1) eliminates this last possibility due to the high absorption required. An alternative giving a chromatic maximum could be the passage of the typical synchrotron frequency in the optical/NIR bands. The time spread for the maximum would depend on the width of the observed frequency band, $t_1/t_2 \propto (\nu_1/\nu_2)^{-2/3}$, with the higher frequencies peaking first. The passage would also produce a spectral change from a positive (1/3) to negative $[-(p-1)/2]$ spectral index in the slow-cooling case (Sari, Piran & Narayan 1998; Chevalier & Li 1999). Again, this is not supported by the data.

The maximum during the early afterglow evolution can then be interpreted as the afterglow onset as for the case of GRB 060418 and GRB 060607A (Jin & Fan 2007; Molinari et al. 2007). Following the formalism reported in equations (1) and (2) of Molinari et al. (2007) in the thin-shell case since the prompt duration was much shorter than the peak of the afterglow emission, we can derive, for GRB 071010A, $\Gamma_0 \approx 150$ for a uniform interstellar medium and $\Gamma_0 \approx 40$ in the case of a wind-shaped density profile. These are lower than the values inferred for GRB 060418 and GRB 060607A due to the late occurrence of the maximum, but still within the theoretical expectations for the external-shock scenario (Sari & Piran 1999; Lithwick & Sari 2001; Zhang et al. 2006).

The observed maximum cannot be related to reverse shock emission. The reverse shock should be in general a short-lasting phenomenon, and in the thin-shell case it should peak slightly before the deceleration time, roughly just before the afterglow onset, and dominate it in case the typical synchrotron emission is close enough to the optical band (Jin & Fan 2007; Kobayashi & Zhang 2007). The rapid decay ($f \sim t^{-2.1}$, Sari & Piran 1999; Kobayashi & Zhang 2007) predicted for the reverse shock emission is inconsistent with the much milder decay observed after the optical flux peak (Table 2).

4.2 The rebrightening

The occurrence of rebrightenings or flares during the temporal evolution of GRB afterglows is not uncommon. The long-time coverage usually provided by the *Swift* XRT affords the study of a large sample of flares from the spectral and energetic (Falcone et al. 2007), or temporal and morphological (Chincarini et al. 2007) points of view. In the optical/NIR the occurrence of large flares seems to be less common, while in a remarkable fraction of cases a rebrightening due to discrete energy injection was included in the modelling (Jóhannesson, Björnsson & Gudmundsson 2006).

Our data set does not permit a detailed analysis of the temporal and spectral evolution of the rebrightening around 0.6 d. The simplest approach is to model the transition as due to the discrete injection of a sizeable amount of energy in the fireball interacting with the external medium by means of refreshed shocks. The flux density produced by an external shock scales with the energy content of the fireball apart from minor differences between the optical/NIR and X-ray bands (Panaitescu & Kumar 2000) which are not detectable in our data. Therefore, to account for the observed $f_{\rm inj}/f \approx 1.9$, an amount of energy comparable to the energy content of the fireball needs to be supplied to the system. Remarkably, a discrete episode of energy injection is not supposed to modify the spectrum of the synchrotron radiation emitted at the shock front if the cooling frequency does not enter or cross the observing bands (Panaitescu & Kumar 2000), in agreement with the achromatic evolution of the afterglow of GRB 071010A. A discrete energy injection, comparable to the energy content of the fireball, was also suggested by de Ugarte Postigo et al. (2007) for GRB 050408. Also in the case of the XRF 050824 a rebrightening was observed at rather late time and a large delayed energy injection was invoked (Sollerman et al. 2007). In principle, a rebrightening could be induced by a density variation in the circumburst medium as proposed by Lazzati et al. (2002) for the GRB 021004 (but see also Nakar & Granot 2007). However, this explanation cannot be applied to our case, since the X-ray range is above the cooling frequency and therefore insensitive to density variations (see e.g. Sari et al. 1998). A transition from wind to homogenous medium, due to the crossing of the wind reverse shock could also generate a rebrightening, as discussed in Pe'er & Wijers (2006). Other explanations are also possible, such as a double jet (Berger et al. 2003) or a patchy shell (Mészáros, Rees & Wijers 1998; Rees & Mészáros 1998). A structured jet with a bright narrow core and fainter wings can also produce a rebrightening close to the jet-break time (Salmonson 2003), though in such a case it would only be due to perspective rather than to real energy injection, possibly driving to a sharp transition if seen from a suitable angle.

Finally, although not required by the data, the temporal profile of the rebrightening is also consistent with that of a fast rise and exponential decay pulse simply superposed on the underlying afterglow. The relatively long duration of the pulse, as compared to the time of occurrence, $\Delta t/t \approx 1$, is compatible with an origin of the emission at the external-shock radius (see discussion in Guetta et al. 2007; Guidorzi et al. 2007a).

4.3 Late-time afterglow, light-curve break and SED analysis

Following the rebrightening at about 0.6 d, the afterglow evolution shows a sharp break at about 1 d consistent with being achromatic in the X-ray and optical/NIR bands (Fig. 2). Following Liang et al. (2008) only seven GRB afterglows have been found so far with such an achromatic transition. Moreover, the general temporal behaviour of the optical/NIR and X-ray light curves seems to be the same, supporting at least qualitatively the possibility that we are observing emission from a single outflow with a transition due to a beamed geometry.

The standard external-shock model predicts specific relations between temporal and spectral parameters. However, it is a well-established observational fact that GRB afterglows show more complex behaviours than expected before the launch of *Swift*. Many mechanisms have been proposed to interpret the new features discovered with *Swift*: delayed energy injection, late central engine activity, refreshed shocks, high-latitude emission, etc. (e.g. Zhang & Mészáros 2004; Zhang et al. 2006). Most of these ingredients affect the light curve shape in a number of ways. However, since the fundamental emission process in the soft X-rays and in the optical/NIR is still synchrotron, the spectra should follow the general predictions of the external-shock scenario. We therefore begin the analysis starting from the broad-band SED from the optical/NIR to the X-rays. The evolution of the afterglow, including the early phases, is consistent with being fully achromatic. We derive the SED at about 0.8 d in order to minimize the need to extrapolate the observations adopting a temporal behaviour (Fig. 3).

The amount of rest-frame neutral absorption required by the X-ray data ($N_{\rm H} \approx 1.7 \times 10^{22}$ cm^{-2}) is within the range observed for a set of well-studied *Swift* GRB X-ray afterglows (Campana et al. 2006). In the optical/NIR the observed SED curvature clearly indicates the need for a substantial absorption, as derived in Section 3, with $E_{\rm B-V} \approx 0.21$ mag. Such an amount of intrinsic absorption in the optical/NIR is uncommon among GRBs with sufficient data quality to allow a meaningful study (see Stratta et al. 2005; Tagliaferri et al. 2006; Kann et al. 2007; Starling et al. 2007, for a comprehensive analysis). As for most of the GRB optical afterglows, a SMC-like extinction curve seems to provide a better fit to the data (Kann, Klose & Zeh 2006; Kann et al. 2007), although the gas-to-dust ratio $N_{\rm H}/E_{B-V}$ is higher than in the SMC, again in agreement with the findings of Starling et al. (2007).

The spectral indices in the optical/NIR and X-ray bands allows us to constrain the electron energy distribution index p ($N \propto \gamma^{-p}$). With the cooling frequency in between the optical/NIR and the X-rays (probably just below the X-ray range, as shown in Fig. 3), we have $\beta_{\rm opt} = (p-1)/2$ and $\beta_{\rm X} = p/2$ and therefore $p_{\rm opt} = 2.52^{+0.46}_{-0.52}$ and $p_{\rm X} = 2.92^{+0.44}_{-0.36}$, independent of the circumburst matter-density profile in the slow-cooling regime (Zhang & Mészáros 2004, and references therein). These values for p, in particular from the X-rays, lie in the high tail of the distribution derived by Tagliaferri et al. (2006) or Shen, Kumar & Robinson (2006), although still consistent with it. The value derived from the optical is also consistent with the typical results ($p \approx 2.2$) of numerical simulations of relativistic shocks (Achterberg et al. 2001; Vietri 2003). Knowing the electron distribution index we can predict the decay rate in the optical/NIR before the occurrence of a jet break, considering also the constraints from the X-rays: $\alpha_{\rm pre,opt} \approx 1.2$–$1.5$ (0.75–1.5 from

the optical/NIR only) in the case of a constant-density radial profile of the circumburst matter, or $\alpha_{\rm pre,opt} \approx 1.7$–$2.0$ (1.25–2.0 from the optical/NIR only) in the case of an environment shaped by a wind from a massive star. For the X-rays (frequencies above the cooling frequency) we have $\alpha_{\rm pre,X} \approx 1.4$–$1.75$ (1.4–2.0 from the X-ray only) independent of the density profile (and unconstrained by our data).

It is clear from the fit results, reported in Section 3 and shown in Fig. 2, that interpreting the break at $\sim$1 d as a jet break, the optical/NIR decay before the transition would be in essential agreement with the expectations for a constant-density medium only for the p value derived from the optical. Otherwise, a continuous additional injection of energy as required by the modelling of numerous *Swift* X-ray afterglows (Panaitescu et al. 2006) should be considered. After the jet break, the decay index in the slow-cooling regime must be the same at all frequencies (higher than the typical synchrotron frequency, as expected $\sim$1 d after the high-energy event), and independent of the circumburst matter-density profile. For $p > 2$, as in our case, it is simply $\alpha_{\rm post} = p$. Again the observed decay indices are consistent with the expectations only with the value derived from the optical/NIR.

In principle, the post-break decay indices would also be consistent with a wind model before the occurrence of a jet break with $p \approx 3.1$. This p value would be better supported by the X-ray spectral data, although the achromaticity of the transition at $\sim$1 d is not consistent with this scenario. The distribution of p values, although likely inconsistent with a unique $p \approx 2.2$ (Shen et al. 2006; Tagliaferri et al. 2006), supports $p < 3$ for essentially all the afterglows once the analysis is based on the spectral parameters rather than on the temporal behaviour.

Summing up, the hypothesis that the sharp achromatic transition at about 1 d be a real jet break appears consistent with the data if we assume that continuous energy injection is affecting the temporal decays. This would be one of the very few instances of a jet break observed both in the optical/NIR and the X-rays. The consistency of the GRB 071010A parameters with the Ghirlanda relation (see below) lends some indirect support to the jet-break interpretation.

After about 10 d the afterglow light curve flattens considerably, plausibly as a result of the emergence of the host-galaxy light. Our data quality does not permit to draw any conclusion about the possible presence of a SN component affecting the light curve and mimic the host-galaxy contribution (see Fig. 2). A SN component comparable to SN 1998bw (Galama et al. 1998) at the redshift of GRB 071010A and including the effect of the fitted absorption in the optical would be in the I band about 0.8 mag fainter than our last measured point.

4.4 Amati and Ghirlanda relations

It is well known that the position of a GRB in the radiated energy versus spectral peak photon energy plane can provide useful clues on the nature, physical origin, and geometry of its emission. Indeed, while all 'normal' long GRBs and XRFs show a clear correlation between these two quantities, short GRBs and peculiar subenergetic GRBs (980425 and, possibly, 031203) show a different behaviour (e.g. Amati 2006). In addition, collimated GRBs seen off-axis are expected to deviate from these spectrum–energy correlations.

The $E_{\rm peak}$ and $E_{\rm iso}$ values derived from the analysis of the time-averaged spectrum (see Section 3) are fully consistent with the $E_{\rm p,i} - E_{\rm iso}$ (Amati) relation (Amati et al. 2002; Amati 2006), showing that the prompt emission of GRB 071010A is not peculiar and indicating that, if the emission is collimated, the off-axis angle is small. In addition, with a break interpreted as a jet break at about 1 d and by assuming, following Ghirlanda et al. (2004), a constant circumburst matter-density profile ($n = 3\,{\rm cm}^{-3}$) and a fireball kinetic to radiated energy conversion efficiency of 0.2, we derive a jet opening angle of $8\overset{\circ}{.}2 \pm 1\overset{\circ}{.}1$ and a collimation-corrected energy of $(3 \pm 2) \times 10^{49}$ erg. Thus, GRB 071010A is also fully consistent with the $E_{\rm p,i} - E_\gamma$ (Ghirlanda) relation (Ghirlanda et al. 2004; Nava et al. 2006). This evidence further supports that the possibly achromatic break observed in the afterglow light curve is due to collimated emission.

Finally, if we fit the time-averaged spectrum of GRB 071010A with a cut-off power law with index fixed at -1, we can constrain the cosmological rest-frame peak energy to 32^{+46}_{-21} keV. This value, combined with the values of $E_{\rm iso}$ and E_γ derived above, make the representative point for GRB 071010A consistent with the best-fitting power law of both the $E_{\rm p,i} - E_{\rm iso}$ and $E_{\rm p,i} - E_\gamma$ relations, thus reinforcing the above considerations.

4.5 Polarization

Almost coincident with the achromatic break, we obtained polarimetric observations, providing a rather robust upper limit (0.9 per cent at 95 per cent, 1.3 per cent at 3σ) suggesting null polarization. Polarimetric measurements of GRB optical afterglows have been performed for several events (Covino et al. 2004). In general, the polarization level was moderate (2–3 per cent), although in a few cases evidence for variations related to the afterglow evolution was found (Bersier et al. 2003; Greiner et al. 2003; Lazzati et al. 2003; Rol et al. 2003; Gorosabel et al. 2004; Lazzati et al. 2004). The simple detection of variable polarization, intrinsically related to the afterglow emission, is still one of the most important observational tests in favour of the external relativistic shock model with physical beaming, where some degree of polarization is naturally expected (Covino et al. 2005; Malesani, Covino & Rossi 2005; Lazzati 2006).

Almost all of the observations have been performed with the goal of disentangling the geometry of the outflow using time-resolved polarimetry. After an initial period of enthusiasm, the required intense and delicate observational efforts and the high degree of complexity of the afterglow light curves provided by *Swift* cast some doubts on the actual possibility of deriving meaningful constraints from simple models (Ghisellini & Lazzati 1999; Sari 1999). These proved to be applicable only to smooth, regular, afterglow light curves. Nevertheless, Rossi et al. (2004) showed that the polarization degree and position angle evolution is strongly dependent on the assumed jet structure. At least in a couple of cases a homogeneous jet geometry could be formally ruled out: i.e. for GRB 020813 (Lazzati et al. 2004) and for GRB 030328 (Maiorano et al. 2006).

The diagnostic power of time-resolved polarimetric observations relies on the strong coupling between the assumed jet geometry and polarization signature. For homogeneous jets there should be two polarization maxima, before and after the jet-break time, with a rotation of the position angle by 90°. For structured jets, (i.e. jets with a more energetic core and fainter wings), the maximum of polarization should almost be coincident with the jet-break time, and the polarization angle constant. Therefore, a polarimetric measurement almost coincident with a jet break, as in the case for GRB 071010A, is of remarkable value. The very low upper limit that we have obtained (Section 3) argues against a structured jet. However, the lack of time-resolved polarimetry through the evolution of the afterglow prevents us from drawing firm conclusions. The polarized fraction for the radiation emitted by an afterglow depends basically on the degree of asymmetry of the system, which in turn depends on the line of sight of the observer with respect to the jet symmetry axis. With a single observation the possibility of a very small offset

angle cannot be ruled out. Setting aside the jet-break hypothesis, it is still true that, whichever physical process is responsible for the (achromatic) steepening observed in the afterglow at about 1 d, it generated radiation with only a very low level of polarization. The same is true if we model the rebrightening at about 0.6 d with a fast rise exponential decline pulse dominating the afterglow luminosity for the pulse duration.

5 CONCLUSION

Our campaign on GRB 071010A is an example of extensive monitoring of a GRB afterglow in the optical/NIR. This allowed us to detect an initial rising phase which can be interpreted as the afterglow onset. The peak time is rather late, about 7 min after the GRB. This would directly imply a relatively small initial Lorentz factor although still within the fireball model expectations. Interesting features are the rebrightening at $\sim$0.6 d followed by an achromatic break $\sim$1 d after the burst. The steepening is observed both in the optical/NIR and in the X-rays bands, a feature seldom observed even in the *Swift* era.

The spectral and temporal relations before and after the break are roughly consistent with the predictions of the afterglow synchrotron external shock model with a cooling break in between the optical/NIR and X-ray bands and assuming also continuous energy injection. The rebrightening episode can be interpreted as being due to the occurrence of a refreshed shock injecting energy in the system comparably to the original energy content of the fireball. Other explanations are still possible, relating the rebrightening to the density profile of the circumburst medium or to structured jets. The optical/NIR SED requires absorption in the host-galaxy satisfactorily modelled with the SMC extinction curve.

GRB 071010A is consistent with the Amati relation and, if the achromatic steepening is interpreted as a jet break, it is consistent with the Ghirlanda relation too. Independent of the emission process, the entire afterglow evolution is consistent with being independent of colour from about 2 min up to a few days. The SED is consistent with synchrotron emission and requires rest-frame absorption both in the X-rays and in the optical/NIR.

We also performed a polarimetric observation almost in coincidence with the occurrence of the achromatic break. A tight (0.9 per cent) upper limit was derived. In the absence of time-resolved polarimetry, we cannot rule out that this afterglow was characterized by a low level of polarization throughout its evolution.

Finally, the rich data set of this burst and the simultaneous availability of multiwavelength data is a positive example of a new approach we are trying to apply to GRBs localized by *Swift*, favouring more complete coverage of a few well-studied GRBs. In addition, the observation of an initial rising phase, a rebrightening episode, and an achromatic break, as well as the availability of a well-sampled broad-band energy distribution, could offer a valuable workbench for alternative interpretative scenarios such as the 'cannonball' (Dado et al. 2008; De Rùjula 2007), the 'fireshell' (Bianco et al. 2008) and the 'quark nova' (Staff, Ouyed & Bagchi 2007) models in order to reach a better understanding of GRB afterglow phenomenology.

ACKNOWLEDGMENTS

SC thanks G. Ghirlanda, G. Ghisellini, D. Malesani and F. Tavecchio for useful discussions. AVF's group at UC Berkeley is funded by NSF grant AST-0607485 and NASA/Swift grant NNG06GI86G. BG acknowledges a post-doctoral grant funded by the Centre National d'Etudes Spatiales. We also thank the anonymous referee for her/his useful comments and suggestions.

REFERENCES

Achterberg A., Gallant Y. A., Kirk J. G., Guthmann A. W., 2001, MNRAS, 328, 393
Amati L., 2006, MNRAS, 372, 233
Amati L. et al., 2002, A&A, 390, 81
Band D. et al., 1993, ApJ, 413, 281
Berger E. et al., 2003, Nat, 426, 154
Berger E. et al., 2006, ApJ, 634, 501
Bersier D. et al., 2003, ApJ, 583, 63
Bertin E., Arnouts S., 1995, A&AS, 177, 393
Beuermann K. et al., 1999, A&A, 352, 26
Bianco C. L., Bernardini M. G., Caito L., Dainotti M. G., Guida R., Ruffini R., 2008, in Bianco C. L., Xue S. S., eds, AIP Conf. Proc. Vol. 966, Relativistic Astrophysics: 4th Italian-Sino Workshop. Am. Inst. Phys. New York, p. 12
Bloom J. S., Perley D. A., Modjaz M., Poznanski D., Chen H.-W., Prochaska J. X., 2007, GCN Circ., 6861
Bringer M., Boër M., Peignot C., Fontan G., Merce C., 1999, A&AS, 138, 581
Burrows D. N., Racusin J., 2006, Nuovo Cimento B, 121, 1273
Calzetti D., Armus L., Bohlin R. C., Kinney A. L., Koornneef J., Storchi-Bergmann T., 2000, ApJ, 533, 682
Campana S. et al., 2006, A&A, 449, 61
Chandra P., Frail D. A., 2007, GCN Circ., 6901
Chevalier R. A., Li Z., 1999, ApJ, 520, 29
Chincarini G. et al., 2007, ApJ, 671, 1921
Conconi P. et al., 2004, in Moorwood A. F. M., Masanori I., eds, Proc. SPIE Vol. 5492, Ground-based Instrumentation for Astronomy. SPIE, Bellingham, p. 1602
Covino S. et al., 1999, A&A, 348, 1
Covino S. et al., 2002, A&A, 392, 865
Covino S. et al., 2003, A&A, 400, 9
Covino S., Ghisellini G., Lazzati D., Malesani D., 2004, in Feroci M., Frontera F., Masetti N., Piro L., eds, ASP Conf. Ser. Vol. 312, Third Rome Workshop on Gamma-Ray Bursts in the Afterglow Era. Astron. Soc. Pac., San Francisco, p. 169
Covino S., Rossi E., Lazzati D., Malesani D., Ghisellini G., 2005, in Burderi L., Antonelli L. A., D'Antona F., Di Salvo T., Israel G. L., Piersanti L., Tornambé A., Straniero O., eds, AIP Conf. Proc. Vol. 797, Interacting Binaries: Accretion, Evolution, and Outcomes. Am. Inst. Phys., New York, p. 144
Covino S., Malesani D., Tagliaferri G., Vergani S. D., Chincarini G., Kann D. A., Moretti A., Stella L., 2006, Nuovo Cimento B, 121, 1171
Curran P. A., van der Horst A. J., Wijers R. A. M. J., 2008, MNRAS, 386, 895
Dado S., Dar A., De Rújula A., 2008, ApJ, 688, 517
Dai X. et al., 2007, ApJL, submitted (arXiv:0712.2239)
De Rùjula A., 2007, preprint (arXiv:0711.0970)
de Ugarte Postigo A. et al., 2007, A&A, 462, 57
Devillard N., 1997, The Messenger, 87
Dickey J. M., Lockman F. J., 1990, ARA&A, 28, 15
Falcone A. D. et al., 2007, ApJ, 671, 1921
Fynbo J. et al., 2007, The Messenger, 130, 43
Galama T. J. et al., 1998, Nat, 395, 670
Gehrels N. et al., 2004, ApJ, 611, 1005
Ghirlanda G., Ghisellini G., Lazzati D., 2004, ApJ, 616, 331
Ghisellini G., Lazzati D., 1999, MNRAS, 309, 7
Gorosabel J. et al., 2004, A&A, 422, 113
Greiner J. et al., 2003, Nat, 426, 157
Greiner J. et al., 2008, PASP, 120, 405
Guetta D. et al., 2007, A&A, 461, 95
Guidorzi C. et al., 2007a, A&A, 474, 793

Guidorzi C., Mangano V., Moretti A., Romano P., 2007b, GCN Circ., 6870
Jakobsson P. et al., 2006, A&A, 447, 897
Jin Z. P., Fan Y. Z., 2007, MNRAS, 378, 1043
Jóhannesson G., Björnsson G., Gudmundsson E. H., 2006, ApJ, 647, 1238
Kann D. A., Klose S., Zeh A., 2006, ApJ, 641, 993
Kann D. A. et al., 2007, ApJ, submitted (arXiv:0712.2186)
Klotz A., Böer M., Atteia J. L., 2007a, GCN Circ., 6860
Klotz A., Böer M., Atteia J. L., 2007b, GCN Circ., 6863
Kobayashi S., Zhang B., 2007, ApJ, 655, 973
Krimm H. et al., 2007, GCN Circ., 6868
Lazzati D., 2006, New J. Phys., 8, 131
Lazzati D., Rossi E., Covino S., Ghisellini G., Malesani D., 2002, A&A, 396, 5
Lazzati D. et al., 2003, A&A, 410, 823
Lazzati D. et al., 2004, A&A, 422, 121
Liang E.-W., Racusin J. L., Zhang B., Zhang B.-B., Burrows D. N., 2008, ApJ, 675, 528
Lithwick Y., Sari R., 2001, ApJ, 555, 540
Maiorano E. et al., 2006, A&A, 455, 423
Malesani D., Covino S., Rossi M., Lazzati D., de Luca A., Filliatre P., Tagliaferri G., 2005, Nuovo Cimento C, 28, 515
Mészáros P., Rees M. J., Wijers R. A. M. J., 1998, ApJ, 499, 301
Molinari E. et al., 2007, A&A, 469, 13
Monet D. G. et al., 2003, AJ, 125, 984
Moretti A., Baumgartner W. H., Gehrels N., Holland S. T., Palmer D. M., Stamatikos M., Ukwatta T. N., 2007, GCN Circ., 6859
Nakar E., Granot J., 2007, MNRAS, 380, 1744
Nava L., Ghisellini G., Ghirlanda G., Tavecchio F., Firmani C., 2006, A&A, 450, 471
Norris J. P., Nemiroff R. J., Bonnell J. T., 1996, ApJ, 459, 393
Nousek J. A. et al., 2006, ApJ, 642, 389
Panaitescu A., 2008, MNRAS, 383, 1143
Panaitescu A., Kumar P., 2000, ApJ, 543, 66
Panaitescu A., Mészáros P., Gehrels N., Burrows D., Nousek J., 2006, MNRAS, 366, 1357
Pe'er A., Wijers R. A. M. J., 2006, ApJ, 643, 1036
Pei Y. C., 1992, ApJ, 395, 130
Perley D. A., Filippenko A. V., Silverman J. M., Foley R. J., Modjaz M., Kocevski D., Bloom J. S., 2007, GCN Circ., 6934
Prochaska J. X., Perley D. A., Modjaz M., Bloom J. S., Poznanski D., Chen H.-W., 2007, GCN Circ., 6864
Rees M. J., Mészáros P., 1998, ApJ, 496, 1
Rol E. et al., 2003, A&A, 405, 23
Rossi E. M., Lazzati D., Salmonson J., Ghisellini G., 2004, MNRAS, 354, 86
Rykoff E. S. et al., 2004, ApJ, 601, 1013
Salmonson J. D., 2003, ApJ, 592, 1002
Sari R., 1999, ApJ, 524, 43
Sari R., Piran T., 1999, ApJ, 520, 641
Sari R., Piran T., Narayan R., 1998, ApJ, 497, 17
Schlegel D. J., Finkbeiner D. P., Davis M., 1998, ApJ, 500, 525
Shen R., Kumar P., Robinson E. L., 2006, MNRAS, 371, 1441
Sollerman J. et al., 2007, A&A, 466, 839
Staff J., Ouyed R., Bagchi M., 2007, ApJ, 667, 340
Starling R. L. C., Wijers R. A. M. J., Wiersema K., Rol E., Curran P. A., Kouveliotou C., van der Horst A. J., Heemskerk M. H. M., 2007, ApJ, 661, 787
Stetson P. B., 1987, PASP, 99, 191
Stratta G., Perna R., Lazzati D., Fiore F., Antonelli L. A., Conciatore M. L., 2005, Nuovo Cimento C, 28, 693
Strutskie M. F. et al., 2006, AJ, 131, 11633
Tagliaferri G. et al., 2006, Nuovo Cimento C, 121, 1163
Vietri M., 2003, ApJ, 591, 954
Vitali F. et al., 2003, in Masanori I., Moorwood A. F. M., eds, Proc. SPIE Vol. 4841, Instrument Design and Performance for Optical/Infrared Ground-based Telescopes. SPIE, Bellingham, p. 627
Zerbi F. M. et al., 2001, Astron. Nachr., 322, 275
Zhang B., Mészáros P., 2004, Int. J. Modern Phys. A, 19, 2385
Zhang B., Fan Y. Z., Dyks J., Kobayashi S., Mészáros P., Burrows D. N., Nousek J. A., Gehrels N., 2006, ApJ, 642, 354

This paper has been typeset from a TEX/LATEX file prepared by the author.